PLASTIC DEFORMATION OF TiAl AND Ti_3Al*

S. M. L. Sastry
McDonnell Douglas Research Laboratories
St. Louis, MO 63166, U.S.A.

H. A. Lipsitt
Metals and Ceramics Division
Air Force Wright Aeronautical Laboratories
Wright Patterson Air Force Base, OH 45433, U.S.A.

1. Introduction

The slip character of titanium-aluminum alloys changes drastically at aluminum concentrations greater than 3-4 at.%. Pure titanium deforms by slip and twinning at low temperatures and predominantly by slip at high temperatures. In Ti-Al alloys, however, with increasing aluminum concentration, twinning is suppressed, and plastic deformation occurs by planar a-slip ($\underline{b} = a/3\ \langle 11\bar{2}0\rangle$) and c-component slip [1-3]. In alloys containing 10 to 20 at.% Al, the compound α_2, based on the composition Ti_3Al and having the DO_{19} type crystal structure, precipitates in the solid solution matrix. Deformation in this class of alloys occurs by the shearing of α_2 precipitates by glide dislocations, leading to the formation of coarse, planar, slip bands. The stress concentrations at slip-band intersections and grain-boundary/slip-band intersections promote cleavage and reduce the ductility and toughness of the alloys. As the aluminum concentration is increased beyond 20 at.%, the directional character of the bonding between Ti and Al atoms increases, and this leads to the formation of the first intermetallic compound Ti_3Al in the Ti-Al system. The second intermetallic compound, which has the $L1_0$-type superlattice structure occurs near 50 at.% aluminum concentration. Because the ordered arrangement of atoms in Ti_3Al and TiAl persists to near the melting temperatures, these compounds have high-temperature strengths and oxidation resistance unequalled by commercial titanium alloys and thus are candidates for high-temperature applications.

The crystal structures of Ti_3Al and TiAl are shown in Figures 1a and 1b. In Ti_3Al, the a-dislocations lying on the basal plane are superlattice dislocations bound by four partial dislocations of the type $a/6\ \langle 10\bar{1}0\rangle$. When slip occurs on prism planes, however, dislocations can travel as unit dislocations without disruption of the ordered arrangement of nearest neighbor atoms. The c+a type activity becomes important at higher temperatures. Although c-type dislocations are observed occasionally, they do not play a major role in the deformation process. In TiAl, the layered arrangement of Ti and Al atoms on successive {100} planes and the slight tetragonality result in nonequivalence of different 1/2 <110> slip vectors. The 1/2 [011] and 1/2 [101] dislocations must move in pairs if the ordered arrangement of atoms is

*This work was performed at the Air Force Wright Aeronautical Laboratories under a grant from the National Research Council.

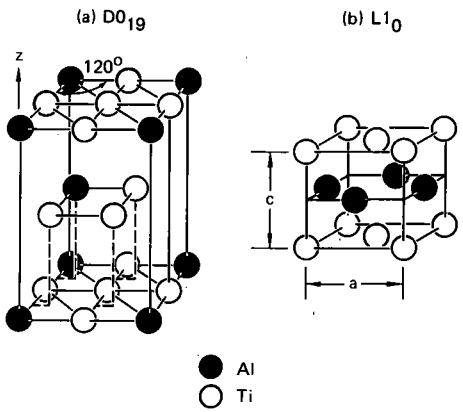

Figure 1. Crystal structures of (a) Ti_3Al and (b) TiAl.

Table 1 Nominal Compositions and Crystal Structures of Titanium Aluminides

Alloy	Crystal Structure
Ti-17Al Ti-16Al-10Nb	Ordered hexagonal close packed DO_{19}
Ti-36Al Ti-36Al-4Nb	Ordered face centered tetragonal $L1_0$

not to be disrupted, whereas the 1/2 [110] dislocations can travel as ordinary unit dislocations without destroying order. Although the possible dislocation configurations in $L1_0$ and DO_{19} superlattices have been known for some time [4,5], detailed investigations of slip systems in TiAl and Ti_3Al have been carried out only recently. The salient features of deformation substructures in Ti_3Al and TiAl at 25-900°C, the role of the unique dislocation configurations of $L1_0$ and DO_{19} superlattices in the development of dislocation substructures, and the consequent effects of substructures on fracture processes are reported here.

2. Experimental Procedure

The nominal compositions of the alloys studied are given in Table 1. The alloys were cast as stick ingots and converted by Nuclear Metals, Inc., to <500-μm size powders using a rotating electrode process. The powders were canned in Ti-6Al-4V cans and hot extruded at 1200-1400°C with an extrusion ratio of 26:1. Cylindrical test specimens having a reduced gauge diameter of 3.6 mm and flanges for clamping the strain measuring device were machined from the extruded rods. The fracture modes and deformation substructures of the specimens deformed at 25-900°C in tension, creep, and fatigue were determined by scanning and transmission electron microscopy.

3. Results

3.1 Mechanical Properties and Deformation Substructures of Ti_3Al and Ti_3Al-Nb

The variations with temperature of tensile and fatigue properties of Ti_3Al are shown in Figure 2. Ti_3Al specimens deformed in uniaxial tension do not exhibit appreciable plastic deformation below 600°C. The high values of tensile and fatigue fracture stresses are retained up to 700°C, with a large decrease in strength occurring only above 800°C. The fatigue ductility (cumulative strain for fracture) is higher than the tensile ductility, and both fatigue and tensile ductilities increase monotonically with temperature up to 700°C. The difference between the tensile and fatigue fracture stresses is less than 8% at temperatures up to 700°C, but the saturation stress in fatigue at 800°C is considerably lower than the tensile fracture stress.

Figure 3 shows the dislocation arrangement on the basal plane of Ti_3Al fractured in tension at 25°C. All the dislocations in Figure 3 have a/3 $\langle 11\bar{2}0 \rangle$ Burgers vectors, and the paired dislocations (as at B) lie on the basal plane, whereas the unit dislocations (shown at P) lie on prism planes in agreement with the predicted dislocation configuration for DO_{19} type superlattices. The c-component dislocations were not observed in specimens deformed at 25°C. Unstable shear containing long pile-ups of dislocations on basal and prism planes was observed in specimens deformed at 25-600°C.

Figure 4 is a comparison of dislocation substructures in Ti_3Al specimens deformed at 700°C in tension, creep, and fatigue. Slip activity occurs on both the basal and prism planes for each mode of deformation. The dominant slip vector in unidirectional deformation is the a-type (Figure 4a). The dislocations are straight, occurring for the most part in a screw orientation, and they are arranged in planar bands. In contrast, the dislocation distribution in specimens deformed in creep at 700°C (Figure 4b) is characterized by a much reduced planarity of slip, a tangled dislocation

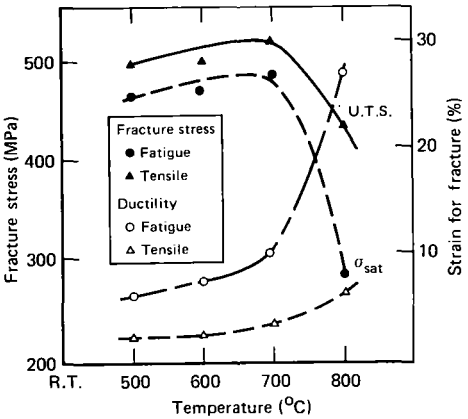

Figure 2. Variation of tensile and fatigue properties with temperature.

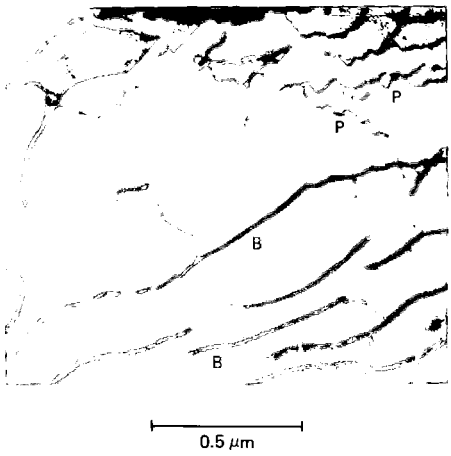

Figure 3. a/3 $<11\bar{2}0>$ {0001} superlattice dislocations and a/3 $<11\bar{2}0>$ {$10\bar{1}0$} unit dislocations in Ti_3Al deformed in tension at 25°C.

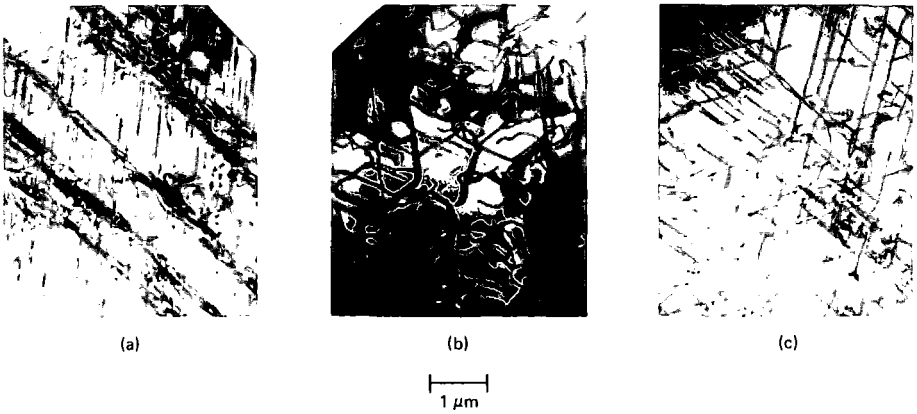

Figure 4. Dislocation substructures on basal planes in Ti_3Al deformed at 700°C; (a) deformed in tension to 3% strain, (b) deformed in creep to 3% strain, and (c) fatigued at $\gamma_p = \pm 0.25\%$, and $\epsilon_{cum} \approx 0.03$.

arrangement instead of planar bands, jogged superlattice dislocations, dislocation loops, and an increased incidence of nonbasal slip vectors. Simple tilt boundaries consisting of one set of superlattice dislocations and mixed tilt-twist boundaries consisting of cross grids of superlattice dislocations were observed in Ti_3Al deformed in creep. In specimens deformed in constant plastic-strain-amplitude fatigue, the type of dislocation structure produced depends on the strain amplitude and cumulative strain. An example of the dislocation structure observed in Ti_3Al fatigued at $\gamma_p = \pm 0.25\%$ to a cumulative strain of 0.03 is shown in Figure 4c. The preferential screw orientation of dislocations is less pronounced in fatigued specimens than in unidirectionally deformed specimens, and many dislocations are arranged in dipole configurations. At higher strain amplitudes and cumulative strains, a dislocation braid structure is developed. The braids are aligned along the traces of the prism and basal planes (Figure 5). The spacing between the braids decreases with increasing strain amplitude.

The c-component dislocations in fatigued Ti_3Al (Figure 6a) are arranged mainly in dipole configurations and are distributed both between the braids and within the braids. In specimens deformed in creep, the c-component dislocations are long and heavily jogged (Figure 6b).

The fracture surfaces of specimens deformed at 25°C and 800°C are shown in Figures 7a and 7b. At 25°C, the fracture is characterized by extensive transgranular cleavage, but at 800°C, the fracture is mixed cleavage, intergranular, and ductile-dimple.

The most important effects of niobium additions to Ti_3Al are to slow the ordering kinetics, reduce the planarity of slip, and increase nonbasal slip activity, all of which result in increased ductility in the niobium-containing specimens. Figure 8b shows the increased c-component dislocation activity in Ti_3Al-Nb compared with Ti_3Al (Figure 8a).

3.2 Mechanical Properties and Deformation Substructures of TiAl and TiAl-Nb Alloys

The temperature dependences of the yield stress and ductility of TiAl are shown in Figure 9. The ratio of fatigue strength (at 10^6 cycles) to the ultimate tensile strength, shown in Figure 10, is significantly higher than that of several other high-temperature materials.

Figure 11 shows the dislocation distribution in a TiAl specimen deformed in tension at 25°C. A detailed Burgers vector analyses of dislocations revealed the activity of predominantly a/2 [110] and a/2 [1$\bar{1}$0] dislocations and a/3 [111] faults. The occurrence of a/2 [101] and a/2 [011] dislocations was rare, and where they were observed occasionally, the superlattice dislocations were pinned by the trailing a/6 [112] partial dislocations.

The most important feature of the dislocation substructure of TiAl deformed in fatigue at room temperature is the presence of a large number of dislocation dipoles and prismatic loops (Figure 12a), which are rare in unidirectionally deformed specimens. The dislocation substructure in specimens fatigued at 800°C (Figure 12b) consists of a well-defined braid structure elongated in the [112] direction and containing edge dislocations and dipoles of all the a/2 <110> Burgers vectors. The regions between the braids contain mainly screw dislocations straddling the braids and edge dislocation dipoles and loops in the process of being swept into the braids. Whereas (111) twinning is the most common twinning mode in both tension and fatigue (Figure 13a), (211) twinning also occurs in fatigued specimens (Figure 13b).

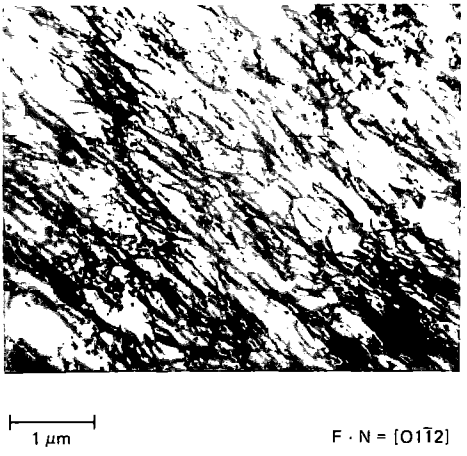

Figure 5. Dislocation arrangement in Ti_3Al fatigued at 700°C at $\gamma_p = \pm 0.125\%$.

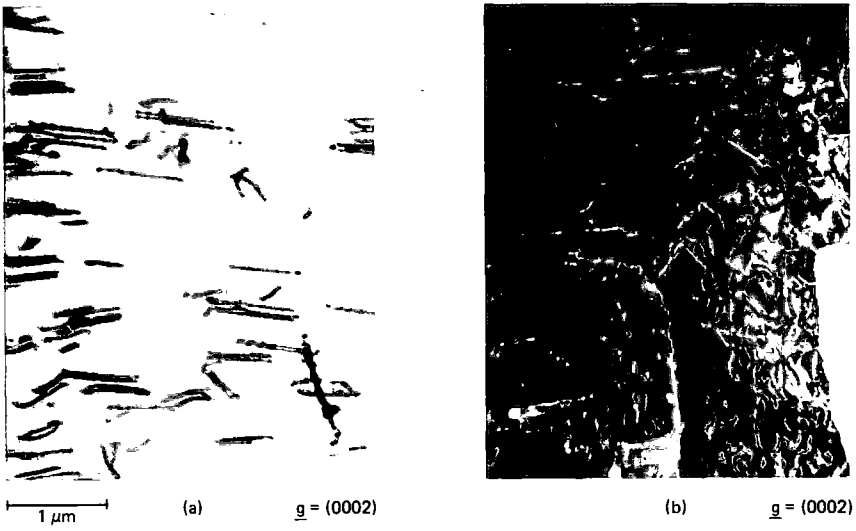

Figure 6. C-component dislocation activity in Ti_3Al; (a) fatigued at 700°C at $\gamma_p = 0.125\%$, $\epsilon_{cum} = 0.05$ and (b) deformed in creep at 700°C to ~5% strain.

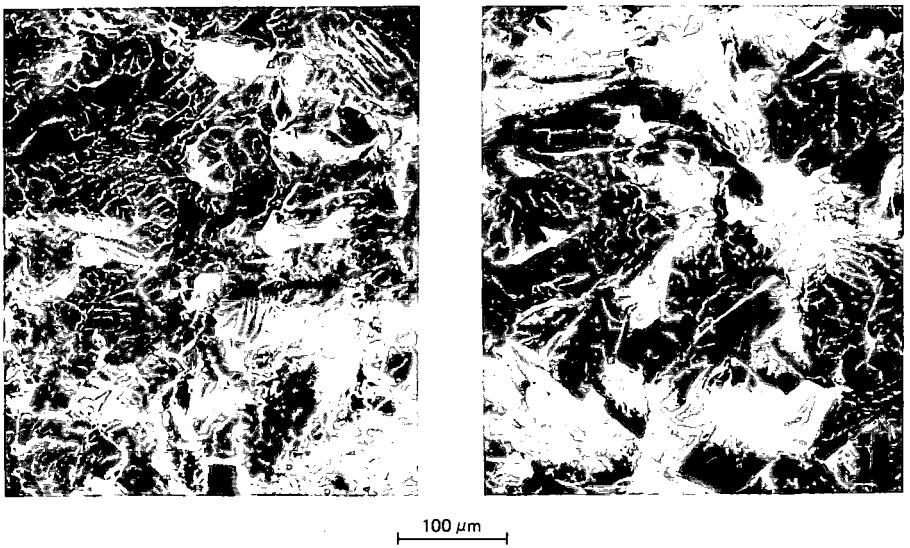

Figure 7. Fracture surfaces of Ti_3Al deformed at (a) 25°C and (b) 800°C.

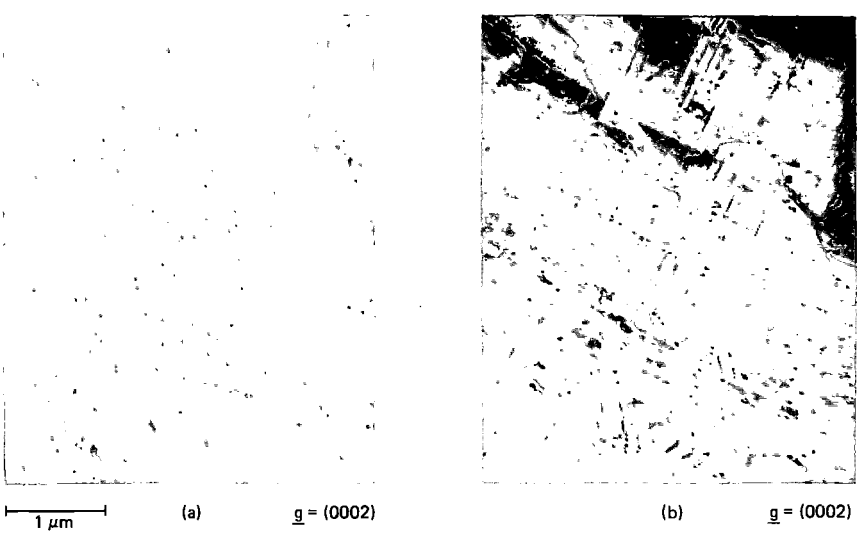

Figure 8. C-component dislocation activity in (a) Ti_3Al and (b) Ti_3Al-Nb deformed in tension at 700°C.

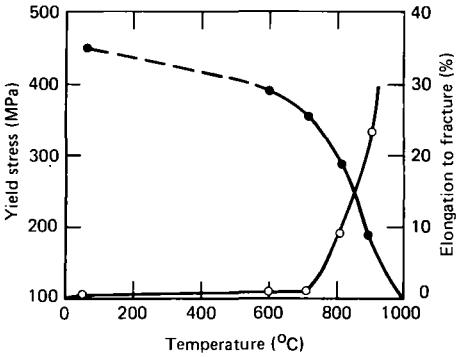

Figure 9. Variation with temperature of yield stress (•) and percentage elongation to fracture (○) of TiAl.

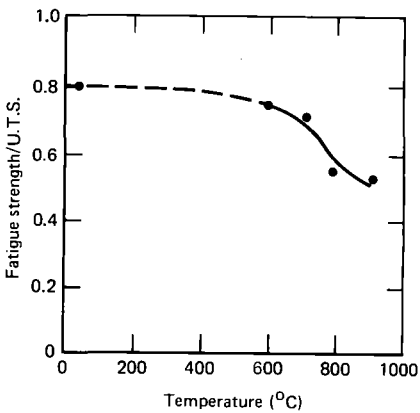

Figure 10. Variation with temperature of fatigue strength to ultimate-tensile-strength (U.T.S.) ratio.

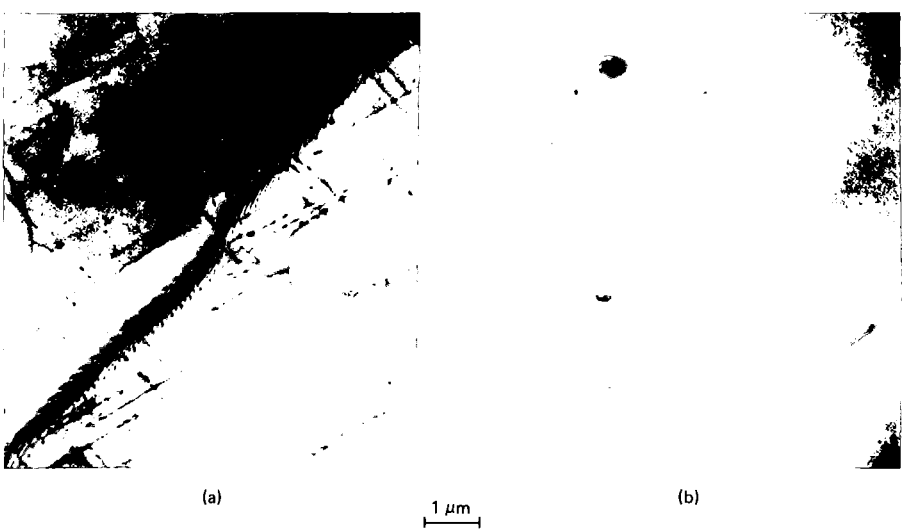

Figure 11. Dislocation structure in TiAl deformed in tension at 25°C; (a) a/2 [110] and a/2 [1$\bar{1}$0] dislocations and (b) a/3 [111] stacking faults.

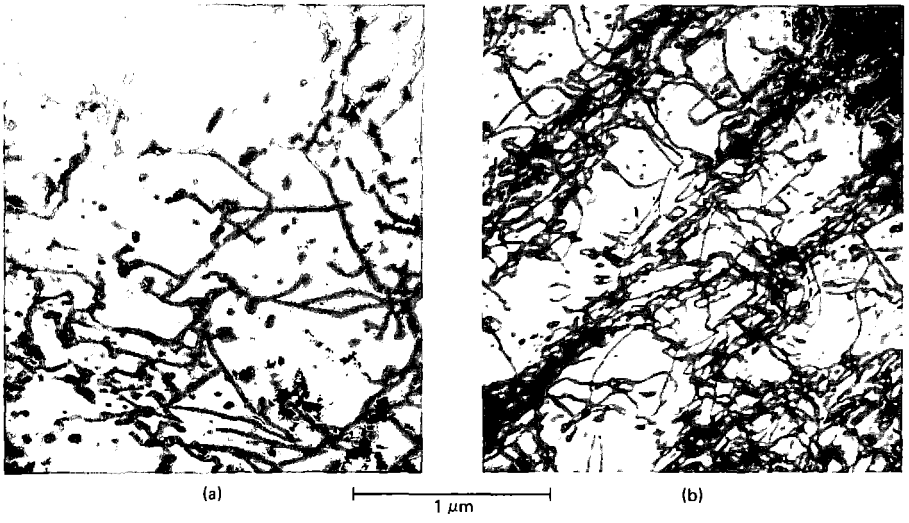

Figure 12. Dislocation substructures in TiAl fatigued at (a) 25°C and (b) 800°C.

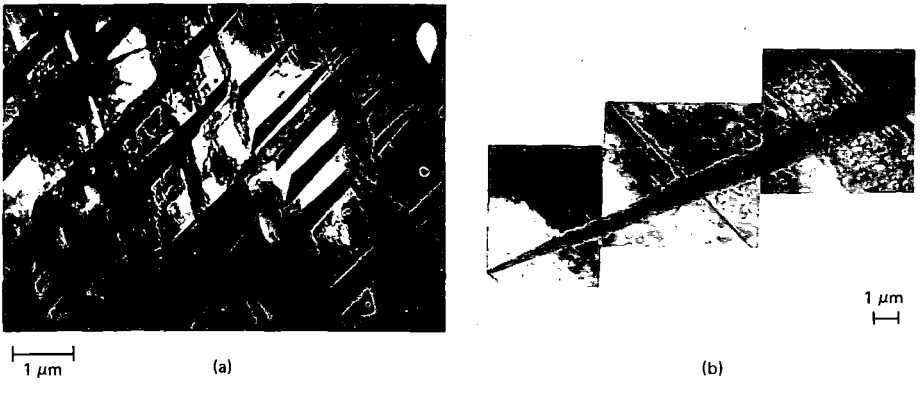

Figure 13. Deformation twins in TiAl (a) {111} twins and (b) {211} twin.

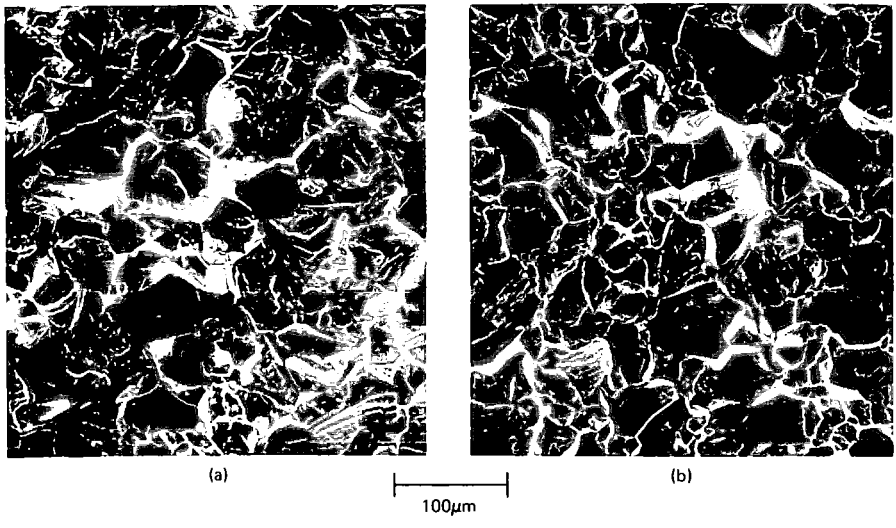

Figure 14. Fracture surfaces of TiAl deformed at (a) 25°C and (b) 800°C.

The fracture surfaces of specimens deformed at 25°C and 800°C are shown in Figures 14a and 14b. At 25°C, fracture occurs by transgranular cleavage. With increasing temperature, the tendency towards intergranular fracture increases, and intergranular fracture dominates at 800°C.

The major influence of niobium additions to TiAl is a lowering of the temperature at which twinning becomes an important mode of deformation and thus a lowering of the ductile-brittle transition temperature of TiAl.

4. Discussion

The dominant mode of slip in Ti_3Al below 700°C is the a-type slip activity. Because of the absence of twinning and c-component dislocation activity, which are required to produce deformation normal to the basal plane, the compound has limited ductility in tension below 700°C. Above 700°C, the activity of nonbasal dislocations combined with the ease of cross slip and climb reduces the work hardening and increases the ductility both in tension and fatigue.

The most striking difference between the deformation substructures of Ti_3Al and other hexagonal close-packed metals and alloys is the absence of twinning in Ti_3Al. This is due to the effect of long range order on suppressing twinning because such deformation in Ti_3Al results in the generation of a net disorder. The dislocation substructure in fatigued Ti_3Al is also considerably different from that observed in fatigued Ti and Mg [6,7]. Whereas walls of edge dipoles are prominent in fatigued Ti and Mg, the dislocations in fatigued Ti_3Al are mostly in a screw orientation, which is characteristic of many ordered structures. Because of the high Peierls' stress in this type of compound, dislocations tend to take up screw orientaions, and the mobility of these dislocations is considerably reduced by directional bonding. Thus, in Ti_3Al, planar bands and dislocation walls, comprised predominantly of a/3 $\langle 11\bar{2}0 \rangle$ screw dislocations are observed up to 700°C. At higher temperatures the mobility of dislocations, is increased because of a reduction in the Peierls' stress and a simultaneous increase in thermally activated cross slip and dislocation climb. These dislocation processes are responsible for the increased ductility of Ti_3Al above 700°C.

In TiAl, the major constraints on plastic flow at low temperatures are the absence of twinning and [011] and [101] type superlattice dislocation activity. The antiphase boundary energy on {111} planes of TiAl is ≈ 0.45 $J \cdot m^{-2}$, and because of directional bonding the lattice friction stress in TiAl is significantly higher than in other face-centered-cubic (f.c.c.) metals and alloys. Furthermore, the effective Burgers vector of superlattice dislocation is twice that of unit dislocation. Consequently, the mobility of superlattice dislocations is greatly reduced because of higher stress required to move superlattice dislocations. The movement of [011] superlattice dislocations is further hindered because of the pinning of the constituent a/6 [112] partial dislocation [8]. The presence of the faulted ribbon bounded by the looped segment of the trailing a/6 [112] partial thus tends to immobilize the three leading partial dislocations. Above 700°C, the a/6 [112] partial is no longer pinned, and the activity of the [011] and [101] superlattice dislocations increases rapidly with increasing temperature. Furthermore, above 700°C, twinning assumes increasing importance as a deformation mode with the concommittant result of increased ductility of TiAl above 700°C.

The dislocation structure in TiAl that has been deformed in fatigue at 700-900°C closely resembles that observed in other f.c.c. metals and alloys,

namely, a dislocation mat structure at small stress amplitudes changing into a closed cell structure at high stress amplitudes. The dislocation braid structure is fully developed near the grain boundaries because of enhanced primary and secondary slip at grain boundaries. This enhanced slip activity at grain boundaries increases the probability that the grain boundaries serve as potential sites for crack nucleation and propagation and hence contribute to intergranular fracture at high temperatures.

5. Summary and Conclusions

The deformation behavior at 25-900°C of TiAl and Ti_3Al was investigated by tensile, creep, and fatigue testing, transmission electron microscopic examination of deformation substructures,and scanning electron microscopic examination of fracture modes. In TiAl, a high Peierls' stress, planar slip, and sessile superlattice dislocation of a/2 [101] and a/2 [011] Burgers' vectors were identified as the sources of low-temperature brittleness. The ductile brittle transition in TiAl occurs at 700°C. The incidence of dislocations of all a/2 <110> slip vectors and {111} <112> twinning results in enhanced ductility above 700°C. The dominant mode of fracture changes from cleavage at room temperature to intergranular above 700°C. In Ti_3Al, the dominant deformation mode at low temperature is a-type [b = 1/3 $\langle 11\bar{2}0 \rangle$] slip activity without any twinning, and fracture is by cleavage. The compound exhibits limited ductility below 700°C. However, in contrast with the abrupt ductile-brittle transition observed at 700°C in TiAl, the ductility of Ti_3Al increases gradually with temperature and remains below that of TiAl at high temperatures. The c+a dislocation activity becomes pronounced above 700°C. Niobium additions to Ti_3Al retard the ordering kinetics, reduce the planarity of slip, and increase nonbasal slip activity. The major influence of niobium additions to TiAl is to lower the temperature at which twinning becomes an important deformation mode and thus lower the ductile-brittle transition temperature of TiAl.

Acknowledgements

The authors gratefully acknowledge the valuable contributions of Drs. M. J. Blackburn, D. Shechtman, R. Schafrik, M. G. Mendiratta, and W. J. Yang and Mr. P. L. Martin to the research described in this paper.

References

1. J. D. Boyd and R. G. Hoagland, in Titanium Science and Technology, Proceedings of Second International Conference on Titanium, ed. by R. I. Jaffee and H. M. Burte, (Plenum Press, New York, 1973), p. 1071.
2. G. Lutjering and S. Weissmann, Acta Met., 18, (1970), p. 785.
3. M. G. Mendiratta, S. M. L. Sastry, and J. V. Smith, J. Mater. Sci., 11, (1976), p. 1835.
4. M. J. Marcinkowski, in Electron Microscopy and Strength of Crystals, ed. by G. Thomas and J. Washburn, (Interscience, New York, 1963), p. 333.
5. M. J. Marcinkowski, N. Brown, and R. M. Fisher, Acta Met., 9, (1961), p. 129.
6. P. G. Partridge, Phil. Mag., 12, (1965), p. 1043.

7. R. Stevenson and J. F. Breedis, Acta Met., 23, (1975), p. 1079.
8. D. Shechtman, M. J. Blackburn, and H. A. Lipsitt, Met. Trans., 5, (1974), p. 1373.